ESTIMATES OF CRUSTAL AND LITHOSPHERIC THICKNESS IN SUB-SAHARAN AFRICA FROM S-WAVE RECEIVER FUNCTIONS

S.E. HANSEN
The Pennsylvania State University, Geosciences Department, 407 Deike Building, University Park
e-mail: shansen@geosc.psu.edu

A.A. NYBLADE
The Pennsylvania State University, Geosciences Department, 446 Deike Building, University Park
e-mail: andy@geosc.psu.edu

J. JULIÀ
The Pennsylvania State University, Geosciences Department, 407 Deike Building, University Park
e-mail: jjulia@geosc.psu.edu

ABSTRACT

Estimates of crustal and lithospheric thickness beneath ten permanent seismic stations in southern, central, and eastern Africa have been obtained from modeling S-wave receiver functions (SRFs). For eight of the examined stations, the Moho depth estimates agree well with estimates from previous studies using P-wave receiver functions (PRFs). For two stations, TSUM and BGCA, previous PRF estimates are not available, and our results provide new constraints on the Moho depth, indicating crustal thicknesses of 35 and 40 km, respectively. SRFs from four stations, BOSA, SUR, FURI, and ATD, display clear S-to-P (Sp) conversions from the lithosphere-asthenosphere boundary (LAB), corresponding to lithospheric thicknesses of 155, 140, 80, and 34 km, respectively. As expected, thicker lithosphere is observed beneath the Precambrian Kaapvaal Craton (station BOSA) and the Namaqua-Natal mobile belt (station SUR) and thinner lithosphere is observed beneath the edge of the Ethiopian rift (station FURI) and the Afar Depression (station ATD). The thinner lithosphere beneath the two latter stations is consistent with the transition from continental to oceanic rifting at the Afar triple junction. For the remaining stations, bootstrap error estimates indicate that the Sp conversion from the LAB cannot be well resolved, calling into question interpretations of lithospheric structure in previous SRF studies using data from these same stations.

Introduction

The depth extent of continental lithosphere beneath Archean and Proterozoic terrains has been debated for many decades (e.g. MacDonald, 1963; Jordan, 1975), and much of this debate has revolved around the nature of the upper mantle structure beneath Africa (Figure 1). Africa is an old continent, much of which was assembled by the mid- to late-Proterozoic, and more recent tectonic activity has only occurred in limited geographic regions. Of all the continents, it has the highest percentage of exposed Precambrian crust (Goodwin, 1996) and therefore provides an important record of Earth's early history.

In southern Africa, the Archean nucleus consists of two main blocks: the Kaapvaal and Zimbabwe Cratons (Figure 1a). The Kaapvaal Craton stabilised by ~2.6 Ga, but the north-central part of the craton was later disrupted (~2.05 Ga) by the Bushveld event, forming the largest known layered mafic intrusion (Von Gruenewaldt et al., 1985). The Zimbabwe Craton stabilised between 2.7 and 3.0 Ga. The two cratons are separated by the Limpopo Belt, which formed in the late Archean when the two cratons collided (De Wit and Roering, 1990). Collectively, the Kaapvaal craton, the Zimbabwe Craton, and the Limpopo Belt form the Kalahari craton, which is bounded to the north, west, and south by a series of Proterozoic mobile belts that sutured to the craton during multiple orogenic events (Figure 1a). Tectonics associated with the Gondwanide orogen in the Proterozoic-Paleozoic led to the formation of the Cape Fold Belt across the southern tip of Africa (Tankard et al., 1982; De Beer and Stettler, 1988; De Wit et al., 1992).

To the northwest, extending into central Africa, is the Congo Craton, which is composed of Archean blocks and early- to mid-Proterozoic fold belts amalgamated during the assembly of Gondwana (Goodwin, 1996; De Waele et al., 2008). Archean crust is exposed in several locations, but the extent of the Congo craton is unknown. In eastern Africa, the Archean Tanzania craton is also surrounded by several Proterozoic mobile belts, including the Ubendian, Kibaran, and Mozambique belts (Figure 1b; Cahen et al., 1984). The most recent tectonics in Africa has also occurred in this area with the development of the Cenozoic East African Rift System. Rifting initiated ~30 to 40 Ma (Burke, 1996) and now extends from north to south along several rift segments from the Afar Depression, through East Africa, and into Mozambique (Figure 1b).

The lithospheric structure of the geologic terrains outlined above has been investigated using a variety of techniques, including body and surface wave

doi:10.2113/gssajg.112.3-4.229

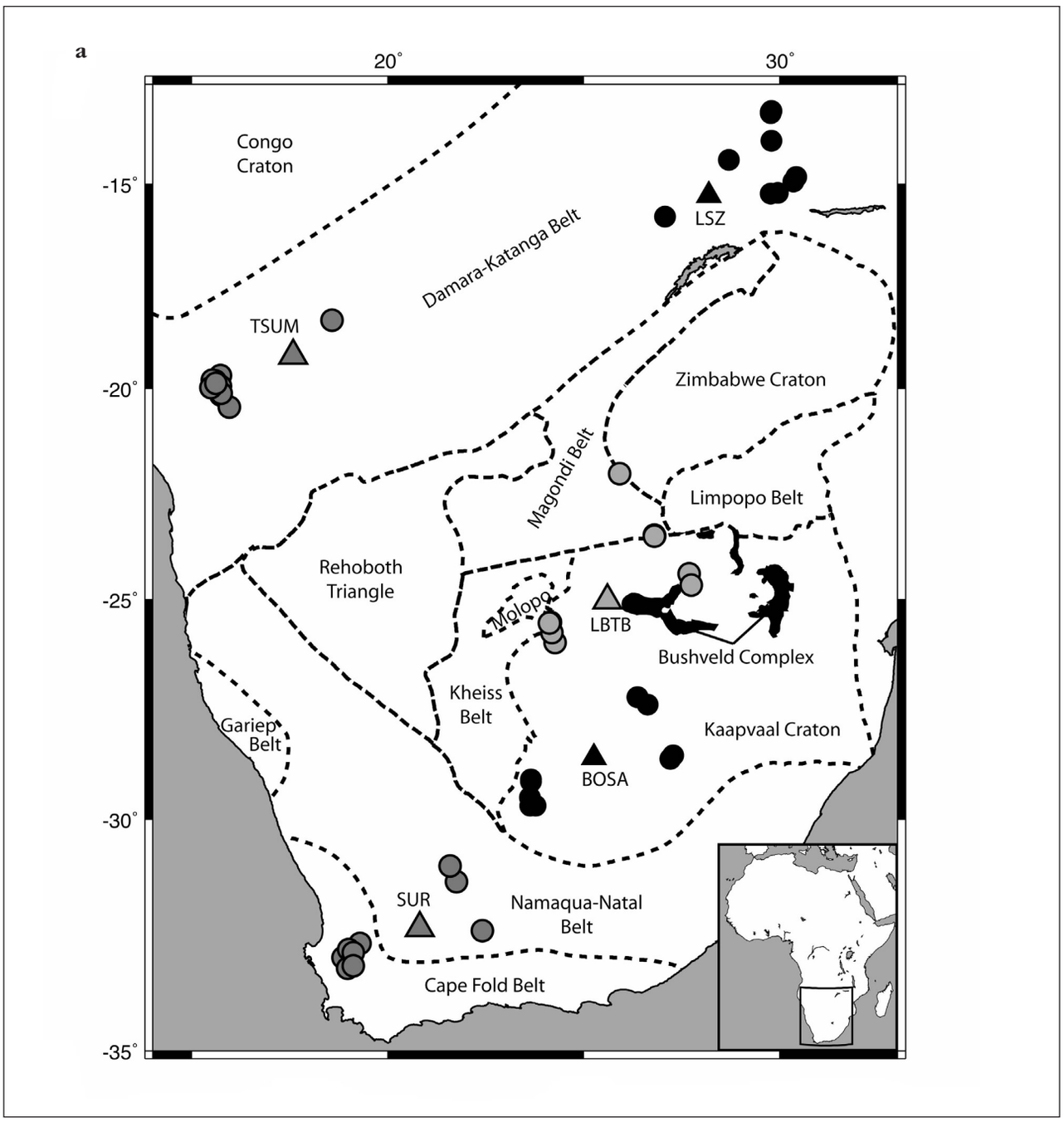

Figure 1. *Stations (triangles) examined in this study in (**a**) southern Africa and (**b**) central and eastern Africa. Note that the two maps are not plotted at the same scale. The Sp conversion points at the best-interpreted LAB depth for each station are shown by circles (BOSA: 155 km, LBTB: 155 km, SUR: 140 km, LSZ: 142 km, TSUM: 180 km, ATD: 34 km, FURI: 80 km, KMBO: 140 km, MBAR: 100 km, BGCA: 285 km). The color shading indicates which Sp conversion points correspond to which station. Bold dashed lines outline the boundaries of labeled tectonic terrains while bold solid lines mark faults and rift segments.*

tomography (James et al., 2001; Fouch et al., 2004; Priestley et al., 2006; 2008; Li and Burke, 2006; Pasyanos and Nyblade, 2007), inversion of surface wave phase velocities (Freybourger et al., 2001; Weeraratne et al., 2003; Larson et al., 2006), regional waveform modeling (Priestley and McKenzie, 2002; Wang et al., 2008), joint inversion of P-wave receiver functions (PRFs) with surface wave dispersion (Julià et al., 2005; Dugda et al., 2007; this volume), thermal estimates based on heat flow data (Jones, 1988; Rudnick and Nyblade, 1999; Artemieva and Mooney, 2001; Deen et al., 2006), and pressure-temperature estimates based on xenolith data (Boyd et al., 1985; Boyd and Gurney, 1986; Deen et al., 2006). Nevertheless, there remain conflicting views on the thickness of the African lithosphere, in part due to previous interpretations of S-wave receiver functions (SRFs; Kumar et al., 2007; Wittlinger and Farra, 2007).

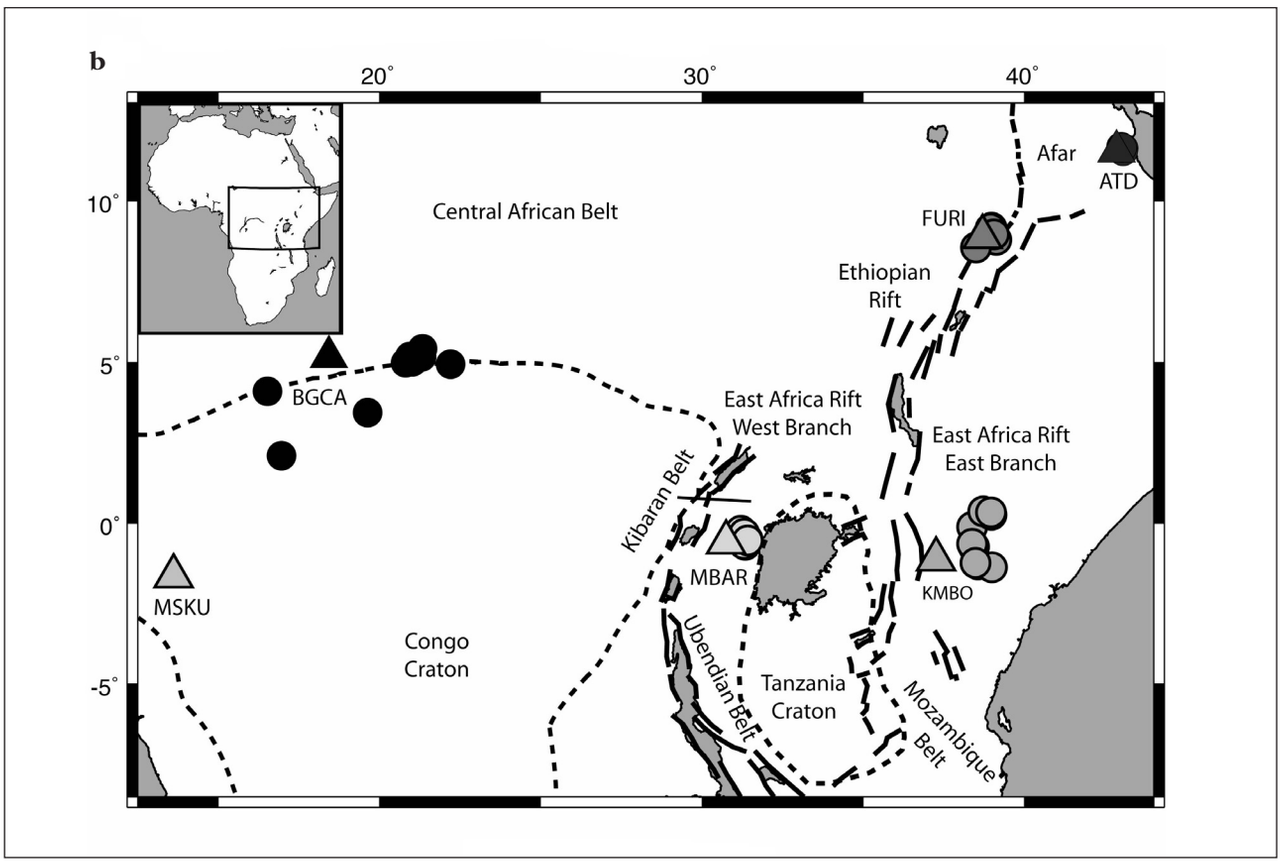

***Figure 1b**. Central and eastern Africa.*

In this study, we also use the SRF technique (e.g. Farra and Vinnik, 2000; Li et al., 2004; Kumar et al., 2007; Hansen et al., 2007; 2009) to investigate the depth of the crust-mantle boundary (Moho) as well as the lithosphere-asthenosphere boundary (LAB) by identifying S-to-P (Sp) conversions from discontinuities beneath several permanent seismic stations in southern, central, and eastern Africa. Unlike PRFs, where crustal multiples can mask conversions from the LAB, boundary conversions on SRFs can be more clearly identified because they arrive earlier than the direct S phase while all crustal multiples arrive later (Figure 2; e.g. Farra and Vinnik, 2000; Li et al., 2004; Kumar et al., 2007; Hansen et al., 2007; 2009). Our SRF analysis differs from previously published studies (Vinnik et al., 2004; Kumar et al., 2007) and provides new estimates of crustal and lithospheric thickness for several terrains in southern, central, and eastern Africa that take into consideration the often large uncertainties associated with SRFs. Our results place new constraints on the nature of the African lithosphere and help to elucidate age-dependent variations in lithospheric structure.

Data and Methodology

Teleseismic waveform data recorded at several permanent stations throughout southern, central, and eastern Africa were used in this study (Figure 1). These stations belong to several networks, including the Global Seismographic Network, the Global Telemetered Seismograph Network, and GEOSCOPE. Most of these stations have been operating since the mid- to late-1990's, providing over ten years of data. To minimize any potentially interfering teleseismic phases (Wilson et al., 2006), we selected S-waves with high signal-to-noise ratios recorded at these stations from earthquakes with magnitudes larger than 5.7, depths less than 250 km, and distances between 60° to 82°. Waveforms were first rotated from the N-E-Z to the R-T-Z coordinate system using the event's back-azimuth and were visually inspected to pick the S-wave onset. The three-component records were then cut to focus on the section of the waveform that is 100 s prior to and 12 s after the S arrival. To detect Sp conversions, the data must be rotated around the incidence angle into the SH-SV-P coordinate system (Li et al., 2004). This second rotation is critical because if an incorrect incidence angle is used, noise can be significantly enhanced and converted phases may become undetectable. To make this second rotation, the approach of Sodoudi (2005) was used to determine the correct incidence angle. The cut R-Z seismograms were rotated through a series of incidence angles to create a set of quasi-SV and quasi-P data. Each quasi-SV component was then deconvolved from the corresponding quasi-P component using Ligorría and Ammon's (1999) iterative time domain method to create a SRF. To make the SRFs

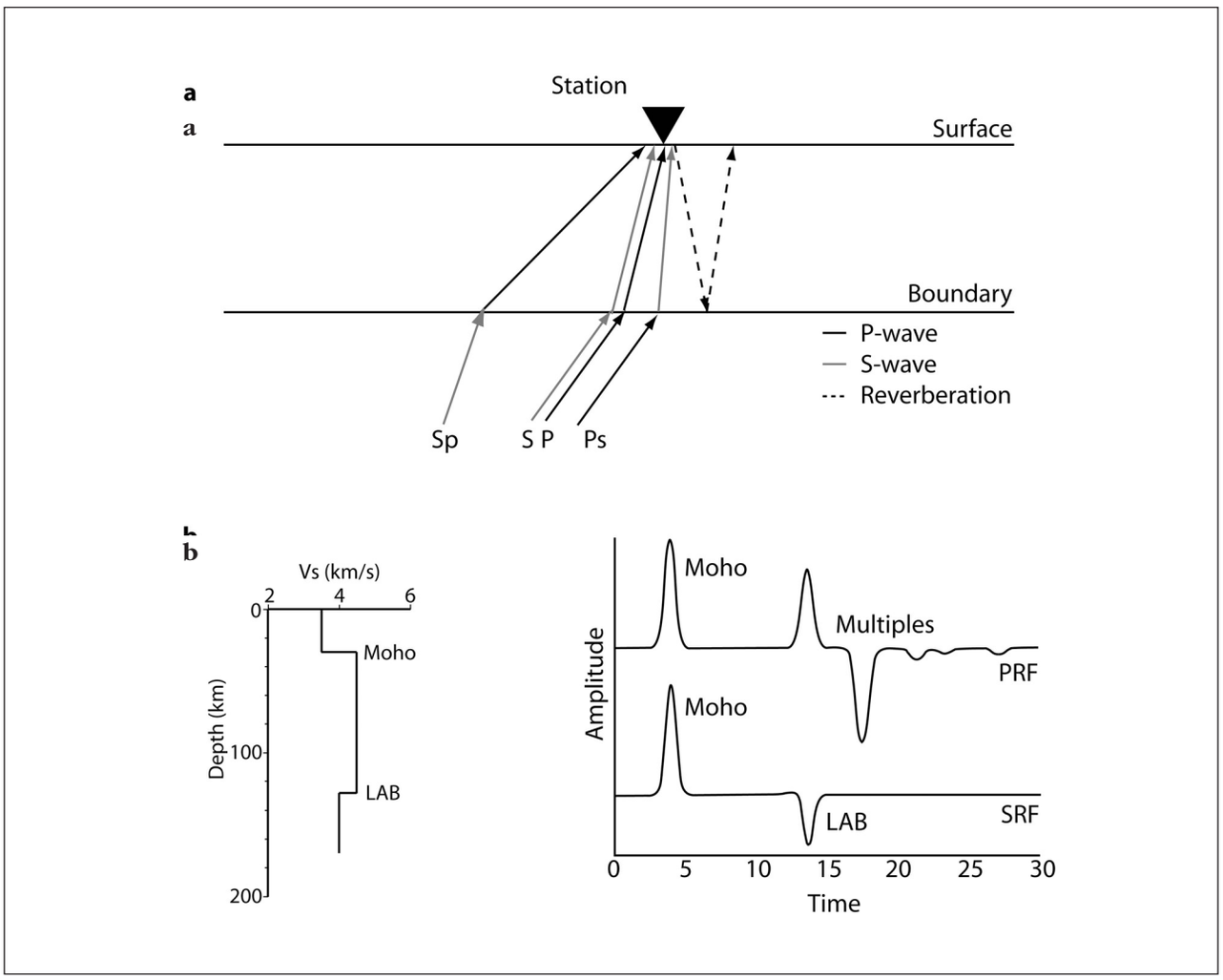

Figure 2. *(**a**) Ray paths of direct P and S phases as well as P-to-S (Ps) and S-to-P (Sp) converted phases. (**b**) Synthetic examples of PRFs and SRFs from the velocity model shown on the left. The time axis and amplitudes of the SRF have been reversed to make the synthetics directly comparable. Note that while the LAB conversion is clear on the SRF, this conversion is masked by crustal multiples on the PRF. Modified from Sodoudi (2005).*

directly comparable to PRFs, both the time axes and the amplitudes of the SRFs were reversed (Figure 2; e.g. Farra and Vinnik, 2000; Li et al., 2004; Kumar et al., 2007; Hansen et al., 2007; 2009). The frequency content of the receiver function is controlled by the Gaussian width factor, *a* (Ligorría and Ammon, 1999). Several values of *a* were examined; however, the best and most consistent results were obtained using an *a* of 1.0.

For a laterally homogenous medium, the optimal incidence angle for rotation into the SH-SV-P coordinate system is the angle that minimises the direct S-wave energy on the P-component. On the time-reversed receiver functions, the direct S arrival is at 0 s. Therefore, the receiver function of interest is the one whose mean amplitude is closest to zero at zero time. All receiver functions for a given event were examined to determine which record best meets this criterion. The P, SV components and the corresponding receiver function with the appropriate incidence angle were retained, and the remaining records were discarded.

Once receiver functions were generated for all events at each station, the dataset was subjected to a number of quality control criteria. First, for stations where PRFs had been previously determined (Midzi and Ottemoller, 2001; Nguuri et al., 2001; Niu and James, 2002; James et al., 2003; Ayele et al., 2004; Dugda et al., 2005; Nair et al., 2006; Stuart et al., 2006; Kgaswane et al., 2008), the SRFs were compared to the PRFs to identify the Moho conversion. Only SRFs that display a clear Moho conversion at the appropriate time were used for further analysis. For the few stations where previously determined PRFs were not available (i.e. TSUM, BGCA), the most consistent, positive conversion on the SRFs was selected as the Moho conversion.

Next, the amplitude of the Moho conversion was examined. Forward modeling was used to predict the expected Moho amplitude using published, averaged velocities for the crust and upper mantle (Niu and James, 2002; Larson et al., 2006; Nair et al., 2006;

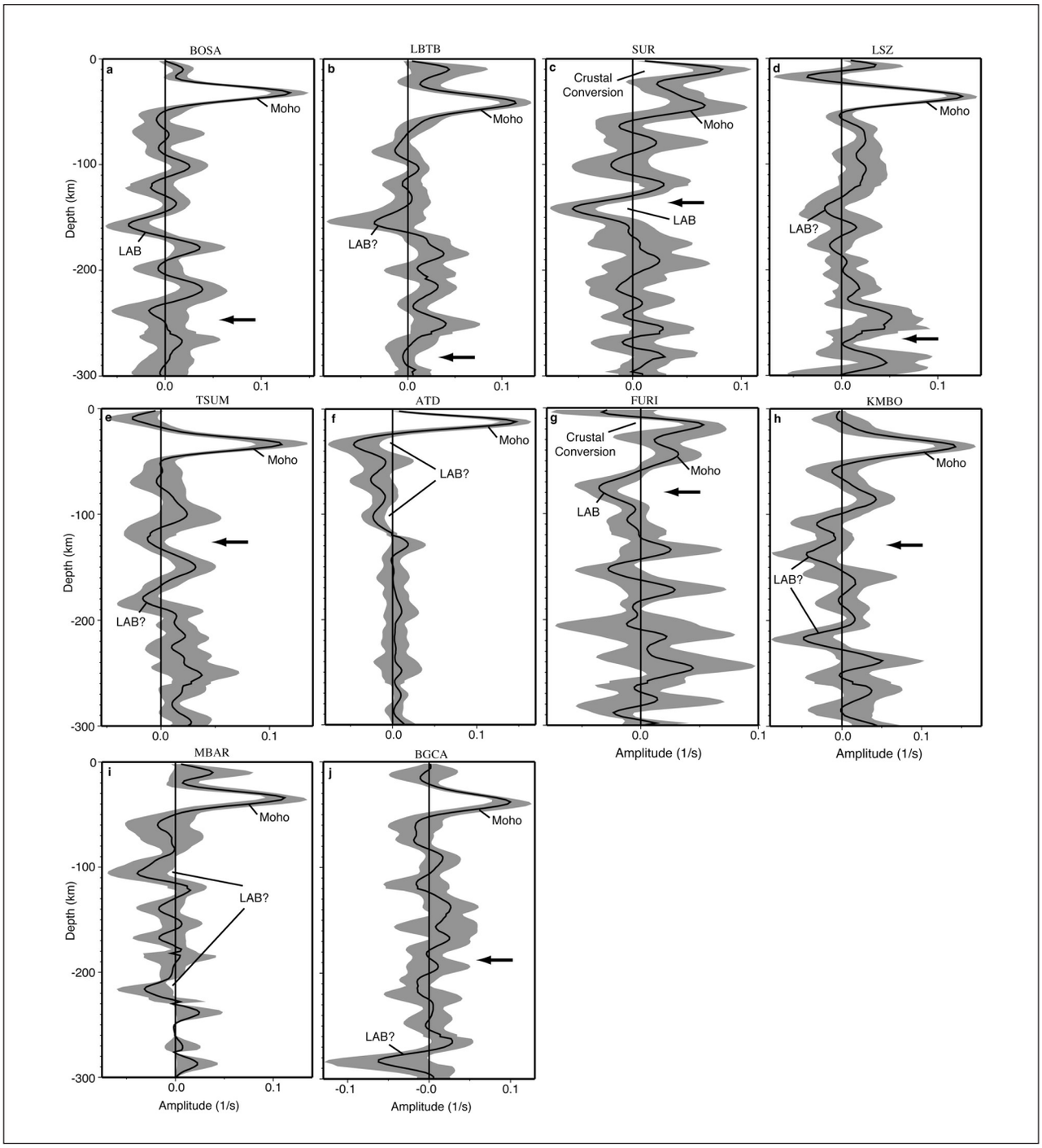

Figure 3. *Stacked SRFs at stations throughout southern, central, and eastern Africa. On each plot, the black line shows the mean stack while the gray shaded areas indicate the 2σ bootstrap error bounds. Major converted phases are labeled. The black arrows indicate LAB depths reported by Kumar et al. (2007) for stations examined in that study.*

Li and Burke, 2006; Wang et al., 2008; Dugda et al., this volume). If the amplitude of the Moho conversion on the SRF was significantly too large or too small (± 3σ), indicating an unrealistic velocity contrast across the crust-mantle boundary, the SRF was discarded. After high-grading the dataset in this manner, we were left with tens of records at each station, representing about 10% of the original dataset. The percentage of useable, high-quality data used in our SRF analysis is comparable to that typically used in previous African PRF studies (e.g. Dugda et al., 2005; Kgaswane et al., 2008); however, fewer events overall were available for SRFs compared to PRFs given the more restricted distance range for events that can be used in the SRF method.

The individual, high quality SRFs were then move-out corrected and stacked using the method of Owens et al. (2000) to improve the signal-to-noise ratio and to

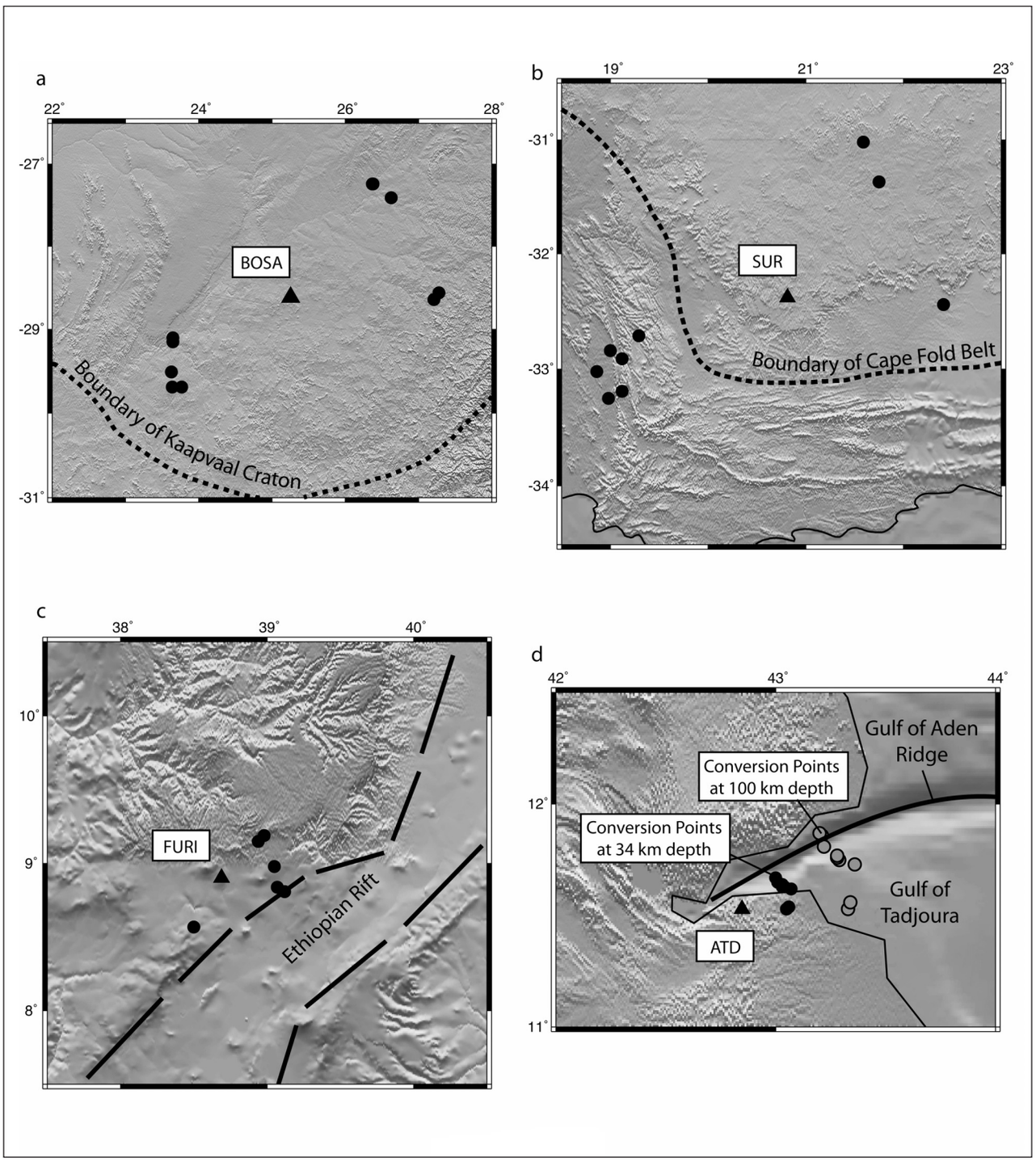

Figure 4. *Maps showing stations (triangles) that have well-resolved SRF LAB signals, in relation to local topography and tectonic features. Topography is taken from the 30 s digital elevation map in GMT (Wessel and Smith, 1998). Bold dashed lines mark terrain boundaries, bold solid lines mark rifts and ridges, and thin solid lines mark the coastline. LAB Sp conversion points are shown by circles. Maps are for stations (**a**) BOSA, (**b**) SUR, (**c**) FURI, and (**d**) ATD.*

convert to depth (Figure 3). A variety of models with crustal and upper mantle velocities appropriate for Africa (Niu and James, 2002; Larson et al., 2006; Nair et al., 2006; Li and Burke, 2006; Wang et al., 2008; Dugda et al., this volume) were examined to optimise the stacks and constrain discontinuity depths; however, the discontinuity depths only varied by about 5 km depending on the choice of model. The final stacks were produced using a modified version of the IASP91 model (Kennett and Engdahl, 1991), with a faster upper crust of 3.5 km/s, more appropriate for Africa (e.g. Nguuri et al., 2001; James et al., 2003; Kgaswane et al., 2008; Dugda et al., this volume). 2σ bootstrap errors for the stack were determined using 200 randomly resampled

sets of the data (Efron and Tibshirani, 1991), which provide further constraints on the SRF depth resolution (Figure 3). For most stations, the Moho depth is resolved to within about ± 4 km, though a few stations have somewhat larger errors (e.g. SUR and FURI). On average, the LAB depth is resolved to within about ± 15 km.

Results

Southern Africa

Stacked SRFs were generated for five stations in southern Africa, including stations BOSA, LBTB, SUR, LSZ, and TSUM (Figure 1a). Station ABPO in Madagascar (not shown) was also examined but since this station has only been operating since April 2007, it has not recorded enough data to meet our event selection criteria. Stations BOSA and LBTB are located in the southern-central and northern Kaapvaal Craton, respectively (Figure 1a). The stacked SRF for station BOSA (Figure 3a) displays a pronounced Moho conversion at 32 km depth, and for station LBTB, a clear Moho conversion is observed at a somewhat deeper depth of 42 km (Figure 3b). Within the associated uncertainty, these crustal estimates match the results of previous studies well (Midzi and Ottemoller, 2001; Nguuri et al., 2001; James et al., 2003; Niu and James, 2002; Nair et al., 2006; Kgaswane et al., 2008). At ~155 km, a trough on the stacked SRF for station BOSA clearly marks the location of the LAB (Figure 3a; Hansen et al., 2009). While a trough is also observed at a similar depth for station LBTB (Figure 3b), this conversion is not as pronounced and falls within the bootstrap error bounds. At the depth of the LAB, the Sp conversion points for station BOSA all fall within the interior of the Kaapvaal Craton, providing good sampling of this terrain (Figures 1a and 4a); however, the conversion points for LBTB are scattered across a variety of geologic boundaries including the Bushveld Complex, the Kaapvaal Craton, the Magondi belt, and the Zimbabwe Craton (Figure 1a). Variable structure between these different terrains may lead to complexity in the stacked SRF, making the LAB conversion less clear.

Station SUR is located within the Proterozoic Namaqua-Natal mobile belt (NNB; Figure 1a), and the stacked SRF for this station displays two crustal conversions, at depths of 10 and 44 km, respectively (Figure 3c). Harvey et al. (2001) and Stankiewicz et al. (2007) imaged a crustal discontinuity beneath this region between 7 to 11 km, similar to the shallower crustal conversion we see on the stacked SRF, and interpreted this feature as a mafic-ultramafic intrusion in the upper crust. A Moho depth of 44 km for the NNB agrees well with previous findings (Nguuri et al., 2001; Nair et al., 2006; Kgaswane et al., 2008) and supports the conclusion that the crust is thinner within the craton (i.e. station BOSA) and thicker within the mobile belts (Nguuri et al., 2001; Niu and James, 2002; James et al., 2003; Kgaswane et al., 2008). A clear LAB conversion at station SUR is observed at ~140 km depth (Figure 3c). It should be noted that while some of the Sp conversion points for events recorded at this station sample the southern NNB at the depth of the LAB, a majority of the conversion points lie beneath the Cape Fold Belt (CFB; Figures 1a and 4b). It has been suggested that the CFB is thrust over the NNB such that both regions are underlain by the same basement structure (Hälbich, 1983). The consistent LAB signal on the stacked SRF may therefore indicate that we are sampling the same NNB lithosphere in both regions.

Stations LSZ and TSUM are located in the Darama-Katanga Belt, which separates the Congo Craton from the Kalahari Craton (Figure 1a). The stacked SRFs for both stations display clear Moho conversions at ~35 km depth (Figures 3d and 3e). Previous crustal thickness estimates in this area are somewhat limited, but Midzi and Ottemoller (2001) estimate the crustal thickness beneath LSZ to be 37 to 44 km, and Pasyanos and Nyblade (2007) report a crustal thickness of 40 to 45 km for the Darama-Katanga belt as a whole. These estimates agree well with our findings. The LAB conversion for stations LSZ and TSUM likely correspond to troughs at 142 and 180 km, respectively, on the stacked SRFs (Figures 3d and 3e); however, in both cases, this signal is on the edge of the bootstrap error limits and is not well resolved.

Eastern Africa

Stacked SRFs were generated for four stations in eastern Africa, including stations ATD, FURI, KMBO, and MBAR (Figure 1b). Station ATD is located within the Afar Depression, on the southern edge of the Gulf of Tadjoura, where the western extension of the Gulf of Aden ridge joins the East African Rift (Figure 4d; Courtillot, 1980; Manighetti et al., 1997). The stacked SRF for this station displays a shallow Moho conversion at ~15 km depth (Figure 3f). Estimates of crustal thickness from previous studies vary significantly beneath this area. Ruegg (1975) interpreted results from a deep seismic sounding experiment in this region and estimated the Moho to be at ~10 km depth. Sandvol et al. (1998) modeled PRFs for crustal structure beneath station ATD and obtained a Moho depth of 8 km. More recently, Dugda and Nyblade (2006) examined crustal structure beneath station ATD using both the H-κ stacking method as well as joint inversion of PRFs and Rayleigh wave group velocities, and they estimate the Moho depth to be 22 to 25 km. Our Moho depth from the stacked SRF falls within these various estimates. Two troughs are also observed on the stacked SRF, at depths of 34 and 100 km, respectively (Figure 3f). While the signal in between these two troughs is at the edge of the noise level, there is some indication of a very broad, negative signal on this section of the stacked SRF. Joint inversion of Rayleigh wave group velocities and PRFs indicate that the lid beneath this area is very thin or nonexistent (Dugda et al., 2007), which is consistent with the shallow (34 km) LAB

conversion observed. The Sp conversion points at 34 km depth lie very close to the Gulf of Aden ridge axis, indicating that these waves are sampling young and presumably thin lithosphere; however, most of the conversion points at 100 km depth lie further off the ridge axis, probably sampling lithosphere that is somewhat older and thicker (Figure 4d). The different pierce points around the ridge axis may lead to the multiple negative conversions observed on the stacked SRF.

Station FURI is located on the northwestern edge of the Ethiopian Rift (Figures 1b and 4c). The stacked SRF for this station displays two crustal conversions, at depths of 16 and 44 km, respectively, and a shallow LAB conversion at ~80 km (Figure 3g). The crustal thickness estimate from the current study agrees well with previously determined PRFs, which indicate a ~40-km thick crust beneath this area (Ayele et al., 2004; Dugda et al., 2005; Stuart et al., 2006). Additionally, joint inversion of Rayleigh wave group velocities and PRFs indicates a thin lithospheric lid beneath this area, extending to a depth of ~70 to 80 km (Dugda et al., 2007), which also agrees well with the stacked SRF at this station.

Station KMBO is located along the Eastern Branch of the East African Rift, and the stacked SRF for this station displays a clear Moho conversion at 36 km depth (Figures 1b and 3h). Previously determined PRFs at this same station indicate a 40 km thick crust (Dugda et al., 2005), agreeing well with our observations. The LAB conversion at this station is less obvious. Two troughs are observed on the stacked SRF at depths of ~140 and ~220 km, respectively (Figure 3h). Joint inversion of PRFs and Rayleigh wave phase and group velocities indicate a lithospheric thickness of ~125 km beneath this region (Dugda et al., this volume), making the shallower trough a more likely candidate as the conversion from the LAB. However, the bootstrap error bounds illustrate that the signal associated with both troughs is close to or below the noise level.

Station MBAR, which is located in the Kibaran mobile belt (Figure 1b), displays a Moho conversion at a depth of 34 km (Figure 3i), agreeing well with previous crustal estimates from PRFs (Dugda et al., 2005). Similar to station KMBO, the stacked SRF for station MBAR also displays two troughs, at depths of ~100 and ~210 km (Figure 3i), making interpretations of the lithospheric thickness less straightforward. It is generally thought that the LAB beneath mobile belts is shallow (Dugda et al., 2007; Priestley et al., 2008), which would better agree with the conversion at ~100 km. However, incoming waves from the east may be sampling the edge of the Tanzania Craton, which is estimated to have a lithospheric thickness of ~200 km (Weeraratne et al., 2003; Pasyanos and Nyblade, 2007; Priestley et al., 2008), making the deeper conversion a more likely LAB signal. In either case, the bootstrap error bounds indicate that this signal is not well resolved.

Central Africa

We examined two stations in central Africa, stations BGCA and MSKU (Figure 1b); however, a stacked SRF could only be generated for BGCA because MSKU has experienced a number of operational problems and has not recorded enough data meeting our event selection criteria. Station BGCA is located on the edge of the Archean Congo craton and the Proterozoic Central African Belt (Figure 1b). The stacked SRF for this station displays a clear Moho conversion at ~40 km depth (Figure 3j). Estimates of crustal thickness in this region of Africa are limited, but the crustal thickness map developed by Pasyanos and Nyblade (2007) shows a ~35 km thick crust in this area, agreeing well with our observation. However, other than the Sp phase from the Moho, most of the other signal on the stacked SRF is within the error estimates. The trough at ~285 km may reflect the LAB signature, corresponding to thick lithosphere beneath the Congo Craton, but the bootstrap errors associated with this signal make such an interpretation uncertain (Figure 3j). Similar to station LBTB in southern Africa, the conversion points for this station are likely spread across various tectonic terrains (Figure 1b), potentially making the LAB signal unclear.

Discussion

Crustal thickness estimates

For most of the stations, crustal thickness estimates have been previously acquired using PRF analysis (Midzi and Ottemoller, 2001; Nguuri et al., 2001; Niu and James, 2002; James et al., 2003; Ayele et al., 2004; Dugda et al., 2005; Nair et al., 2006; Stuart et al., 2006; Kgaswane et al., 2008), and we find that our SRFs produce comparable results. Most previous studies in Africa have focused on upper mantle structure beneath the Kalahari craton in southern Africa or beneath the rift system in eastern Africa, and therefore published estimates of crustal thickness beneath other portions of the continent, such as beneath stations TSUM and BGCA, are limited to interpretations from continental-scale crustal thickness maps generated from the inversion of surface wave dispersion measurements with periods less than ~35 s (e.g. Pasyanos and Nyblade, 2007). Consequently, our SRF results provide new constraints on the crustal thickness for these regions. Both stations TSUM and BGCA are located within Proterozoic mobile belts (Figure 1), and their Moho depths (TSUM: ~35 km; BGCA: ~40 km) are somewhat deeper than that observed within the Kaapvaal Craton (e.g. BOSA: ~30 km), perhaps reflecting differences in the crustal formation process between Archean and post-Archean time (Nguuri et al., 2001; Niu and James, 2002; James et al., 2003; Kgaswane et al., 2008).

Crustal and lithospheric thickness comparison to other SRFs

As part of their study, Kumar et al. (2007) generated SRFs for eight of the 12 stations we have examined

(stations BOSA, BGCA, FURI, KMBO, LBTB, LSZ, SUR, and TSUM). In most cases, the crustal thickness estimates from their study are comparable to our findings; however, two stations provide notable exceptions. For stations FURI and SUR, Kumar et al. (2007) report crustal thicknesses of 16 and 32 km, respectively. In contrast, our stacked SRFs at both of these stations display multiple crustal conversions (Figures 3c and 3g). For station FURI, we also observe an Sp conversion at 16 km but believe that the Moho corresponds to the deeper conversion at 44 km. This observation is consistent with Moho depth estimates from previously determined PRFs (Dugda et al., 2005; Ayele et al., 2004; Stuart et al., 2006). Additionally, wide-angle seismic reflection/refraction profiles (e.g. Mechie and Prodehl, 1988; Mackenzie et al., 2005; Maguire et al., 2006), geochemical analysis (Rooney et al., 2008), and a recent gravity survey (Cornwell et al., 2006) in the vicinity of station FURI also indicate a 40 to 45 km thick crust. Similarly, station SUR displays a crustal thickness of ~44 km, which again is also consistent with estimates from previous PRF studies (Nguuri et al., 2001; Nair et al., 2006).

The LAB interpretations between our study and Kumar et al. (2007) are more varied. Of the eight stations common to both studies, our bootstrap errors indicate that a clear LAB signal can only be interpreted at stations FURI, SUR, and BOSA, which display lithospheric thicknesses of about 80, 140, and 155 km, respectively. Kumar et al. (2007) report similar lid thicknesses for FURI and SUR, with LAB depths of 80 and 134 km, respectively. However, for station BOSA, they report a significantly deeper LAB at 257 km. The trough they interpreted as the LAB conversion at BOSA falls within the bootstrap error bounds on our stacked SRF (Figure 3a; Hansen et al., 2009).

At the remaining five stations, the LAB estimates from Kumar et al. (2007) range from 123 km (station KMBO) to 293 km (station LBTB). However, given our bootstrap error estimates, we believe that these observations are not well resolved as our stacked SRFs show no clear indication of a LAB signature at the depths they reported for these stations (Figure 3). The distribution of LAB conversion points and error estimates for the SRFs were not included in their study, making their contoured interpretation of the lithospheric thickness beneath Africa difficult to assess (Figure 4 from Kumar et al., 2007).

Wittlinger and Farra (2007) also used SRFs to examine multiple Sp conversions beneath the Kaapvaal Craton. They interpreted a trough at ~350 km on their stacked SRFs as the LAB while a shallower trough at ~160 km (similar to that seen in our results for station BOSA) is interpreted as being the base of an anisotropic region in the upper mantle. However, their LAB-interpreted trough is only resolved within a 1σ uncertainty level and both isotropic and anisotropic velocity models predict comparable SRFs (Figure 4d-e in Wittlinger and Farra, 2007). Additionally, Wittlinger and Farra (2007) incorporated events with epicentral distances up to 110° in their analysis, which may be contaminated by other teleseismic phases (Wilson et al., 2006), and mixed events whose Sp conversion points sample different tectonic terrains.

In another study, Vinnik et al. (2004) used the SRF method to investigate the lithospheric structure near station ATD in Afar. They identify a Moho Sp conversion at ~20 km depth, comparable to our result for this station, as well as an additional Sp conversion at ~160 km depth with a polarity similar to that of the Moho conversion. To model their SRFs, Vinnik et al. (2004) require a low-velocity zone between about 100 to 150 km depth, and the Sp conversion at ~160 km coincides with the base of this layer. We also observe a positive Sp conversion on our stacked SRF for station ATD, though at a somewhat shallower depth of ~130 km (Figure 3). However, this feature is at the limit of our resolution and is therefore not interpreted. Vinnik et al. (2004) do not interpret a LAB conversion; however, side lobes on the Moho Sp conversion introduced by their methodology may make such a conversion difficult to discern. Additionally, in their study, Vinnik et al. (2004) incorporate data with average epicentral distances up to 90°. Again, using events with greater epicentral distances such as these may contaminate the SRFs with other teleseismic phases, making interpretation more difficult (Wilson et al., 2006). It is interesting, however, that the top of the low-velocity zone in their models corresponds well with the negative conversion at ~100 km depth on our stacked SRF for this station.

Lithospheric thickness comparison to other studies

Since our bootstrap error estimates indicate that a clear LAB signal can only be interpreted at stations BOSA, SUR, FURI, and ATD, the results from these four stations will be compared to previous studies. In the southern-central Archean Kaapvaal Craton, station BOSA displays a LAB conversion at ~155 km depth (Figures 1a, 3a, and 4a). The lithospheric thickness estimate from the SRF analysis agrees well with previous studies. Using Rayleigh wave tomography, Li and Burke (2006) imaged a fast mantle lid beneath the southern and central Kaapvaal Craton to an average depth of 180 ± 20 km. Priestley et al. (1999; 2006; 2008), who examined multi-mode high frequency surface wave data, report a 160 to 170 km thick lid beneath this region. Regional waveform modeling also indicates that the thickness of the lithosphere beneath southern Africa does not exceed 160 km (Priestley and McKenzie, 2002). These lithospheric thickness estimates also agree well with those inferred from heat flow and from pressure-temperature approximations based on kimberlite nodule data, which place the lid thickness at 150 to 170 km (Jones, 1988; Rudnick and Nyblade, 1999; Artemieva and Mooney, 2001; Deen et al., 2006; Priestley et al., 2006). The Kaapvaal Craton may not be indicative of Archean terrains in general as its lithospheric thickness may be

thinner than other African cratons, like the West African and Congo Cratons (Artemieva and Mooney, 2001; Pasyanos and Nyblade, 2007; Priestley et al. 2008). This area of southern Africa is also marked by anomalously high surface topography (Nyblade and Robinson, 1994), and it is possible that the mechanisms leading to these high elevations may have also altered the local lithospheric structure (Hansen et al., 2009).

Station SUR, located in the southern Proterozoic NNB, displays a LAB conversion at ~140 km depth (Figures 1a, 3c, and 4b). Estimates of the lithospheric thickness from other seismic investigations are somewhat limited in this region, but Li and Burke (2006) estimate the lid thickness in the NNB to only be 80 ± 20 km. Even when considering the error bounds, this is thinner than our estimate. However, the lithospheric thickness estimates from the SRF analysis agree well with other types of data. Artemieva and Mooney (2001) used heat flow measurements to estimate the lithospheric thickness for various Precambrian terrains and reported a thickness of 100 to 140 km for the NNB. Geotherms derived from xenolith pressure and temperature data also indicate a ~140 km thick lithosphere beneath the NNB (Boyd et al., 1985; Boyd and Gurney, 1986). It is interesting that the lid thickness in this area is fairly comparable to that observed in the Kaapvaal Craton since the lithospheric thickness within the mobile belts is often thought to be much thinner (e.g. Priestley et al., 2008). As mentioned previously, the NNB may have been overthrust by the CFB, leading to thicker lithosphere in this region of the mobile belt (Figure 4b; Hälbich, 1983).

Stations FURI and ATD are located on the northwestern edge of the Ethiopian rift and within the Afar Depression, respectively (Figures 1b, 4c, and 4d), and both stations display shallow LAB conversions (Figures 3f and 3g). As mentioned previously, joint inversion of Rayleigh wave group velocities and PRFs indicates a thin lithospheric lid beneath station FURI, extending to a depth of ~70 to 80 km, with an even thinner or nonexistent lid beneath station ATD (Dugda et al., 2007). Similar findings have also been made by other seismic studies, and it is generally accepted that the upper mantle beneath the Ethiopian rift and Afar has been thermally modified by a mantle plume, leading to lithospheric thinning, flood basalt volcanism, and regional uplift (e.g. Debayle et al., 2001; Bastow et al., 2005; 2008; Benoit et al., 2006). Interestingly, the extent of lithospheric thinning is much greater than the corresponding crustal thinning in this region. Modeling of wide-angle seismic reflection/refraction data (Maguire et al., 2006) and inferred composition from Poisson's ratio estimates (Dugda et al., 2005; Stuart et al., 2006) indicate the presence of mafic crust in the Ethiopian Rift, extending northward into Afar. As proposed by Ebinger and Casey (2001), rifting and extensional strain in the crust appears to be accommodated by mafic intrusions.

Conclusion

We have used SRFs in an attempt to further quantify the crustal and lithospheric thickness beneath various terrains in southern, eastern, and central Africa. Where available, the crustal estimates from our SRF analysis agree well with those made in previous studies. For two stations, TSUM and BGCA, our SRF analysis provides new constraints on the Moho depth in these regions. For the ten stations where stacked SRFs could be generated, only stations BOSA, SUR, FURI, and ATD display clear LAB signatures. The corresponding lithospheric thicknesses are consistent with their respective geologic regions, highlighting structure beneath the Kaapvaal Craton, the Namaqua-Natal mobile belt, the Ethiopian Rift, and the Afar Depression. For the remaining stations, bootstrap error estimates indicate that the LAB conversion is difficult to discern, calling into question interpretations put forth in previous SRF studies of the lithospheric structure beneath these stations.

Acknowledgements

We thank Ian Bastow and an anonymous reviewer for their thorough critiques of this manuscript. Support for this work has been provided by the National Science Foundation, grant number E-530062. Figures were prepared using GMT (Wessel and Smith, 1998).

References

Artemieva, I.M. and Mooney, W.D. (2001). Thermal thickness and evolution of Precambrian lithosphere: A global study. *Journal of Geophysical Research*, **106**, 16387–16414.

Ayele, A., Stuart, G. and Kendall, J. (2004). Insights into rifting from shear wave splitting and receiver functions; an example from Ethiopia. *Geophysical Journal International*, **157**, 354–362.

Bastow, I.D., Stuart, G.W., Kendall J.M. and Ebinger, C.J. (2005). Upper-mantle seismic structure in a region of incipient continental breakup; northern Ethiopian Rift. *Geophysical Journal International*, **162**, 479–493.

Bastow, I.D., Nyblade, A.A., Stuart, G.W., Rooney, T.O. and Benoit, M.H. (2008). Upper Mantle Seismic Structure beneath the Ethiopian Hotspot: Rifting at the Edge of the African Low Velocity Anomaly. *Geochemistry, Geophysics, and Geosystems*, **9**, doi: 10.1029/2008GC002107.

Benoit, M.H., Nyblade, A.A. and VanDecar, J.C. (2006). Upper mantle P-wave speed variations beneath Ethiopia and the origin of the Afar hotspot. *Geology*, **34**, 329–332.

Boyd, F.R., Gurney, J.J. and Richardson, S.H. (1985). Evidence for a 150–200 km thick Archean lithosphere from diamond inclusion thermobarometry. *Nature*, **315**, 387–389.

Boyd, F.R. and Gurney, J.J. (1986). Diamonds and the African lithosphere. *Science*, **232**, 472–477.

Burke, K. (1996). The African Plate. *South African Journal of Geology*, **99**, 339–410.

Cahen, L., Snelling, N.J., Delhal, J. and Vail, J.R. (1984). *The Geochronology and Evolution of Africa*. Oxford University Press, New York.

Cornwell, D.G., Mackenzie, G.D., England, R.W., Maguire, P.K.H., Asfaw, L.M., and Oluma, B. (2006). Northern Main Ethiopian Rift crustal structure from new high-precision gravity data, *In:* G. Yirgu, C.J. Ebinger, and P.K.H. Maguire (Editors) The Afar volcanic province within the East African Rift system. *Geological Society of London Special Publications*, **259**, 307–321.

Courtillot, V. (1980). Opening of the Gulf of Aden and Afar by progressive tearing. *Physics of the Earth and Planetary Interiors*, **21**, 343–350.

Debayle, E., Leveque, J.J. and Cara, M. (2001). Seismic evidence for a deeply rooted low-velocity anomaly in the upper mantle beneath the northeastern Afro/Arabian continent. *Earth and Planetary Science Letters*,

193, 423–436.

De Beer, J.H. and Stettler, E.H. (1988). Geophysical characteristics of the southern African continental crust. *Journal of Petrology Special Volume*, 163–184.

Deen, T., Griffin, W., Begg, G., O'Reilly, S., Natapov, L. and Hronsky, J. (2006). Thermal and compositional structure of the subcontinental lithospheric mantle: Derivation from shear wave seismic tomography. *Geochemistry, Geophysics, and Geosystems*, **7**, doi: 10.1029/2005GC001120.

De Waele, B., Johnson, S.P. and Pisarevsky, S.A. (2008). Palaeoproterozoic to Neoproterozoic growth and evolution of the Western Congo Craton: Its role in the Rodinia puzzle. *Precambrian Research*, **160**, 127–141.

De Wit, M.J and Roering, C. (1990). The Limpopo Belt, *In:* J.M. Barton (Editor), A Field Workshop on Granulites and Deep Crustal Tectonics, Extended Abstracts, *Rand Afrikaans University, Johannesburg, South Africa*, 42–52.

De Wit, M.J., Roering, C., Hart, R.J., Armstrong, R.A., de Ronde, C.E.J., Green, R.W.E., Tredoux, M., Peberdy, E. and Hart, R.A. (1992). Formation of an Archean continent. *Nature*, **357**, 553–562.

Dugda, M.T., Nyblade, A.A., Julià, J., Langston, C.A., Ammon, C.J. and Simiyu, S. (2005). Crustal structure in Ethiopia and Kenya from receiver function analysis: Implications for rift development in eastern Africa. *Journal of Geophysical Research*, **110**, doi:10.1029/2004JB003065.

Dugda, M.T. and Nyblade, A.A. (2006). New constraints on crustal structure in eastern Afar from the analysis of receiver functions and surface wave dispersion in Djibouti, *In:* G. Yirgu, C.J. Ebinger, and P.K.H. Maguire (Editors), The Afar Volcanic Province within the East African Rift System, *Geological Society Special Publications*, **259**, 239–251.

Dugda, M.T., Nyblade, A.A. and Julià, J. (2007). Thin lithosphere beneath the Ethiopian Plateau revealed by a joint inversion of Rayleigh wave group velocities and receiver functions. *Journal of Geophysical Research*, **12**, doi:10.1029/2006JB004918.

Ebinger, C. and Casey, M. (2001). Continental breakup in magmatic provinces: An Ethiopian example. *Geology*, **29**, 527–530.

Efron, B. and Tibshirani, R. (1991). Statistical data analysis in the computer age. *Science*, **253**, 390–395.

Farra, V. and Vinnik, L. (2000). Upper mantle stratification by P and S receiver functions. *Geophysical Journal International*, **141**, 699–712.

Fouch, M., James, D., VanDecar, J., van der Lee, S. and the Kaapvaal Seismic Group (2004). Mantle seismic structure beneath the Kaapvaal and Zimbabwe cratons. *South African Journal of Geology*, **107**, 33–44.

Freybourger, M., Gaherty, J., Jordan, T. and the Kaapvaal Seismic Group (2001). Structure of the Kaapvaal craton from surface waves. *Geophysical Research Letters*, **28**, 2489–2492.

Goodwin, A.M. (1996). *Principles of Precambrian Geology*, Academic Press, San Diego, Californa, United States of America, 327pp.

Hälbich, I.W. (1983). Disharmonic folding, detachment, and thrusting in the Cape Fold Belt, *Special Publications of the Geological Society of South Africa*, **12**, 115–123.

Hansen, S.E., Rodgers, A.J., Schwartz, S.Y. and Al-Amri, A.M.S. (2007). Imaging ruptured lithosphere beneath the Red Sea and Arabian Peninsula. *Earth and Planetary Science Letters*, **259**, 256–265.

Hansen, S.E., Nyblade, A.A., Julià, J., Dirks, P.H.G.M. and Durrheim, R.J. (2009). Upper Mantle Low-Velocity Zone Structure beneath the Kaapvaal Craton from S-wave Receiver Functions, *Geophysical Journal International*, (in press).

Harvey, J.D., De Wit, M.J., Stankiewicz, J. and Doucouré, C.M. (2001). Structural variations of the crust in the Southwest Cape, deduced from seismic receiver functions. *South African Journal of Geology*, **104**, 231–242.

James, D., Fouch, M., VanDecar, J., van der Lee, S. and the Kaapvaal Seismic Group (2001). Tectospheric structure beneath southern Africa. *Geophysical Research Letters*, **28**, 2485–2488.

James, D., Niu, F. and Rokosky, J. (2003). Crustal structure of the Kaapvaal Craton and its significance for early crustal evolution. *Lithos*, **71**, 413–429.

Jones, M. (1988). Heat flow in the Witwatersrand Basin and environs and its significance for the South African shield geotherm and lithosphere thickness. *Journal of Geophysical Research*, **93**, 3243–43260.

Jordan, T. (1975). The continental tectosphere, *Reviews in Geophysics*, **13**, 1–12.

Julià, J., Ammon, C.J. and Nyblade, A.A. (2005). Evidence for mafic lower crust in Tanzania, East Africa, from joint inversion of receiver functions and Rayleigh wave dispersion velocities. *Geophysical Journal International*, **162**, 555–569.

Kennett, B. and Engdahl, E. (1991). Traveltimes for global earthquake location and phase identification. *Geophysical Journal International*, **105**, 429–465.

Kgaswane, E., Nyblade, A., Dirks, P., Pasyanos, M., Julià, J. and Durrheim, R. (2008). Crustal Structure of Southern Africa. *EOS Transactions, American Geophysical Union*, **89**, S23A–1866.

Kumar, P., Yuan, X., Ravi Kumar, M., Kind, R., Li, X. and Chadha, R. (2007). The rapid drift of the Indian tectonic plate. *Nature*, **449**, 894–897.

Larson, A., Snoke, J. and James, D. (2006). S-wave velocity structure, mantle xenoliths, and the upper mantle beneath the Kaapvaal Craton. *Geophysical Journal International*, **167**, 171–186.

Li, X., Kind, R., Yuan, X., Wolbern, I. and Hanka, W. (2004). Rejuvenation of the lithosphere by the Hawaiian plume. *Nature*, **427**, 827–829.

Li, A. and Burke, K. (2006). Upper mantle structure of southern Africa from Rayleigh wave tomography. *Journal of Geophysical Research*, **111**, doi:10.1029/2006JB004321.

Ligorría, J. and Ammon, C. (1999). Poisson's ratio variations of the crust beneath North America. *Seismological Research Letters*, **70**, 274pp.

MacDonald, G. (1963). The deep structure of continents, *Reviews in Geophysics*, **1**, 587–665.

Mackenzie, G.D., Thybo, H. and Maguire, P.K.H. (2005). Crustal velocity structure across the Main Ethiopian Rift: results from two-dimensional wide-angle seismic modeling. *Geophysical Journal International*, **162**, 994–1006.

Maguire, P.K.H, Keller, G.R., Klemperer, S.L., Mackenzie, G.D., Keranen, K., Harder, S., O'Reilly, B., Thybo, H., Asfaw, L., Khan, M.A. and Amha, M. (2006). Crustal structure of the northern Main Ethiopian Rift from the EAGLE controlled-source survey; a snapshot of incipient lithospheric break-up, *In:* G. Yirgu, C.J. Ebinger, and P.K.H. Maguire (Editors), The Afar volcanic province within the East African Rift system, *Geological Society of London Special Publications*, **259**, 269–291.

Manighetti, I., Tapponnier, P., Courtillot, V., Gruszow, S. and Gillot, P.Y. (1997). Propagation of rifting along the Arabia-Somalia plate boundary: The gulfs of Aden and Tadjoura. *Journal of Geophysical Research*, **102**, 2681–2710.

Mechie, J. and Prodehl, C. (1988). Crustal and uppermost mantle structure beneath the Afro-Arabian rift system. *Tectonophysics*, **153**, 103–121.

Midzi, V. and Ottemoller, L. (2001). Receiver function structure beneath three Southern Africa seismic broadband stations. *Tectonophysics*, **339**, 443–454.

Nair, S., Gao, S., Liu, K. and Silver, P. (2006). Southern African crustal evolution and composition: Constraints from receiver function studies. *Journal of Geophysical Research*, **111**, doi:10.1029/2005JB003802.

Nguuri, T., Gore, J., James, D., Webb, S., Wright, C., Zengeni, T., Gwavava, O., Snoke, J. and Kaapvaal Seismic Group (2001). Crustal structure beneath southern Africa and its implications for the formation and evolution of the Kaapvaal and Zimbabwe cratons. *Geophysical Research Letters*, **28**, 2501–2504.

Niu, F. and James, D. (2002). Fine structure of the lowermost crust beneath the Kaapvaal craton and its implications for crustal formation and evolution. *Earth and Planetary Science Letters*, **200**, 121–130.

Nyblade, A. and Robinson, S. (1994). The African Superswell. *Geophysical Research Letters*, **21**, 765–768.

Owens, T., Nyblade, A., Gurrola, H. and Langston, C. (2000). Mantle transition zone structure beneath Tanzania, East Africa. *Geophysical Research Letters*, **27**, 827–830.

Pasyanos, M.E. and Nyblade, A.A. (2007). A top to bottom lithospheric study of Africa and Arabia. *Tectonophysics*, **444**, 27–44.

Priestley, K. (1999). Velocity structure of the continental upper mantle: evidence from Southern Africa. *Lithos*, **48**, 45–56.

Priestley, K. and McKenzie, D. (2002). The structure of the upper mantle beneath Southern Africa. *Geological Society Special Publications*, **199**, 45–64.

Priestley, K., McKenzie, D. and Debayle, E. (2006). The state of the upper mantle beneath southern Africa. *Tectonophysics*, **416**, 101–112.

Priestley, K., McKenzie, D., Debayle, E. and Pilidou, S. (2008). The African upper mantle and its relationship to tectonics and surface geology. *Geophysical Journal International*, **175,** 1108–1126.

Rooney, T., Hanan, B., Furman, T. and Graham, D. (2008). Multi-component isotopic mixing in the Ethiopian Rift; modeling plume contributions to recent magmatism. *Geochimica et Cosmochimica Acta*, **72**, A804pp.

Ruegg, J.C. (1975). Main results about the crustal and upper mantle structure of the Djibouti region (T.F.A.I.), *In:* A. Pilger and A. Rosler (Editors). Afar Depression of Ethiopia, *E. Schweizer. Verlagsbuchhandl. (Naegele u. Obermiller), Stuttgart, Federal Republic of Germany (DEU),* 120–134.

Rudnick, R. and Nyblade, A. (1999). The thickness and heat production of Archean lithosphere: constraints from xenolith thermobarometry and surface heat flow, *In:* Y. Fei, C. Bertka, and B. Mysen (Editors). Mantle Petrology: Field Observations and High Pressure Experimentation: A Tribute to Francis R. (Joe) Boyd, *Special Publication of the Geochemistry Society*, **6**, 3–12.

Sandvol, E., Seber, D., Calvert, A. and Barazangi, M. (1998). Grid search modeling of receiver functions; implications for crustal structure in the Middle East and North Africa. *Journal of Geophysical* Research, **103**, 26899–26917.

Sodoudi, F. (2005). Lithospheric structure of the Aegean obtained from P and S receiver functions, *Unpublished PhD Thesis, Freie Universitat Berlin, Germany*, 166pp.

Stankiewicz, J., Ryberg, T., Schulze, A., Lindeque, A., Weber, M.H. and De Wit, M.J. (2007). Results from wide-angle seismic refraction lines in the southern Cape. *South African Journal of Geology*, **110**, 407–418.

Stuart, G.W., Bastow, I.D. and Ebinger, C.J. (2006). Crustal structure of the northern Main Ethiopian Rift from receiver function studies, *In:* G. Yirgu, C.J. Ebinger, and P.K.H. Maguire (Editors), The Afar volcanic province within the East African Rift system, *Geological Society of London Special Publications*, **259**, 253–267.

Tankard, A.J., Jackson, M.P., Eriksson, K.A., Hobday, D.K., Hunter, D.R. and Minter, W.E. (1982). Crustal Evolution of Southern Africa: 3.8 Billion Years of Earth History, *Springer Publishing, New York, United States of America,* 523pp.

Vinnik, L., Farra, V. and Kind, R. (2004). Deep structure of the Afro-Arabian hotspot by S receiver functions. *Geophysical Research Letters*, **31**, doi:10.1029/2004GL019574.

Von Gruenewaldt, G., Sharpe, M.R. and Hatton, C.J. (1985). The Bushveld Complex; introduction and review. *Economic Geology*, **80**, 803–812.

Wang, Y., Wen, L. and Weidner, D. (2008). Upper mantle SH- and P-velocity structures and compositional models beneath southern Africa. *Earth and Planetary Science Letters*, **267**, 596–608.

Wittlinger, G. and Farra, V. (2007). Converted waves reveal a thick and layered tectosphere beneath the Kalahari super-craton, *Earth and Planetary Science Letters*, **254**, 404–415.

Weeraratne, D., Forsyth, D., Fischer, K. and Nyblade, A. (2003). Evidence for an upper mantle plume beneath the Tanzanian craton from Rayleigh wave tomography. *Journal of Geophysical Research*, **108**, doi:10.1029/2002JB002273.

Wessel, P. and Smith, W. (1998). New, improved version of the Generic Mapping Tools Released. *EOS Transactions, American Geophysical Union*, **79**, 579pp.

Wilson, D., Angus, D., Ni, J. and Grand, S. (2006). Constraints on the interpretation of S-to-P receiver functions. *Geophysical Journal International*, **165**, 969–980.

Editorial handling: R.J. Durrheim